


Article

A Formation Control and Obstacle Avoidance Method for Multiple Unmanned Surface Vehicles

Guanqun Liu , Naifeng Wen, Feifei Long and Rubo Zhang *

College of Mechanical and Electrical Engineering, Dalian Minzu University, Dalian 116600, China; liuguanqun@dlmu.edu.cn (G.L.); wennaifeng@dlmu.edu.cn (N.W.); dqpilf@126.com (F.L.)

* Correspondence: zhangrubo@dlmu.edu.cn

Abstract: This study introduces a method for formation control and obstacle avoidance for multiple unmanned surface vehicles (USVs) by combining an artificial potential field with the virtual structure method. The approach involves a leader–follower formation structure, where the leader autonomously avoids collisions using an artificial potential field based on the target’s position as a reference. It also determines the ideal position of each follower in the formation based on its own position, heading angle, and the formation structure. To effectively avoid obstacles and maintain formation, the follower selects the position of the target or its ideal position as a reference during movement, depending on whether it is being repelled by obstacles. Additionally, this paper modifies the attractive force model of the traditional artificial potential field method to restrict the maximum magnitude of the attractive force when encountering repulsive forces, thus expediting departure from obstacle areas. The dynamic characteristics of USVs are taken into account by constraining the maximum linear speed and angular speed. Formation stability is ensured by maintaining a constant speed for the leader, while the linear speed of the follower varies based on the distance to the reference object during movement. Simulation experiments demonstrated that this method can effectively avoid obstacles and maintain formation.

Keywords: unmanned surface vehicle; obstacle avoidance; formation maintenance; artificial potential field; virtual structure



Citation: Liu, G.; Wen, N.; Long, F.; Zhang, R. A Formation Control and Obstacle Avoidance Method for Multiple Unmanned Surface Vehicles. *J. Mar. Sci. Eng.* **2023**, *11*, 2346. <https://doi.org/10.3390/jmse11122346>

Academic Editors: Carlos Guedes Soares, Sergei Chernyi and Weicheng Cui

Received: 1 November 2023
Revised: 5 December 2023
Accepted: 8 December 2023
Published: 12 December 2023



Copyright: © 2023 by the authors. Licensee MDPI, Basel, Switzerland. This article is an open access article distributed under the terms and conditions of the Creative Commons Attribution (CC BY) license (<https://creativecommons.org/licenses/by/4.0/>).

1. Introduction

USVs can be deployed in hazardous situations to perform specialized tasks, thereby minimizing potential casualties. They can also be utilized for monotonous and repetitive tasks, effectively reducing the workload on humans. In extreme marine environments, the capabilities of a single USV may not be sufficient. Therefore, it becomes necessary to integrate multiple USVs into a cluster, to tackle complex tasks through information integration. A cluster of USVs have stronger perception ability, larger operating range, and stronger risk resistance compared to a single USV [1]. Multiple USVs can be effectively deployed in complex and hazardous water areas where manned vessels cannot be dispatched or where individual USVs may not be able to complete tasks. These areas could include high-risk environments or areas contaminated by nuclear, biological, or chemical agents [2]. Multiple-USV collaborative formation operations are capable of performing a wide range of tasks, including coastal patrols and maritime rescue, without endangering the safety of naval personnel.

A cluster of USVs can be regarded as a multi-agent system, which refers to a system composed of multiple interacting agents that can jointly complete certain tasks [3]. In a multiple-USV system, each USV has a certain range of perception ability and can independently perform relatively simple tasks. When faced with complex tasks, they need to collaborate in order to complete the task. This collaboration typically requires information sharing and task allocation. For example, in a USV formation collision avoidance mission,

each USV in the formation provides information support for optimized path planning and formation maintenance by sharing their respective perceived information. Usually, the information will be gathered by the USV designated as the leader. The leader makes collision avoidance decisions and updates the formation based on global information, and sends these decisions and formation information to the members of the formation [4–6].

In multi-agent systems, the collaborative formation is a fundamental issue as it plays a decisive role in efficiently executing specific tasks [7–9]. Formation collision avoidance aims to guide a group of USVs to form specific geometric configurations and control the motion of the formation. In the past few decades, collaborative formation research has mainly focused on unmanned aerial vehicles and intelligent robots, with relatively few studies on collaborative formation of USVs. With the expansion of the application range of USVs, research on the collaboration of multiple USVs has received much attention. Researchers have gradually deepened their research on formation control, continuously improving the performance of formation control algorithms, making multiple-USV formations suitable for various marine environments. The main problems for collaboration among multiple USVs include collaborative collision avoidance, formation, intersection, etc. [10]. Basic formation control approaches include behavior-based methods, virtual structure methods, artificial potential field methods, graph theory methods, and leader–follower methods [11].

The complex and dynamic marine environment, along with the presence of moving obstacles, presents significant challenges in designing formation control strategies. Factors such as the interference of wind, waves, and water flow, particularly the resistance of water, further complicate the problem. Many scholars have considered the effects of these interferences in the research of multiple-USV collaborative formations [12]. With the development of artificial intelligence, biomimetic optimization algorithms and artificial intelligence methods based on learning and gaming have made significant progress [4,13–15]. As a type of ship, USVs must comply with maritime traffic regulations in practical applications. The Convention on International Regulations for Preventing Collisions at Sea (COLREGs) stipulates the navigation rules that all ships must comply with at sea to prevent collisions. To expand the application range of USVs, scholars have introduced COLREGs into the research of USV technology. Kim [16] proposed a distributed local search algorithm to achieve multiple-ship formations and a distributed random search algorithm to reduce the amount of information transmission among multiple ships, thereby adjusting the formation faster. Ma [17] proposed quantitative standards for a wide range of complex collision avoidance situations involving a large number of USVs under COLREGs.

While researchers have conducted extensive research about USV formations and obtained promising results, the pursuit of simple and effective methods has always been a primary goal. Given the challenges of obstacle avoidance and formation maintenance, this paper uses an artificial potential field for collision avoidance and the virtual structure method for formation maintenance. The formation control adopts the leader–follower method. The leader independently avoids collisions based on the artificial potential field, using the position of the target as attractor, and generates the ideal position of each follower in the formation based on its own position, heading angle, and the formation structure. The follower selects the position of the target or its ideal position as the attractor during movement based on whether it is being repelled by obstacles or not. In order to quickly leave the obstacle area, this paper modified the attractive force model of the traditional artificial potential field (APF). This includes a limitation on the maximum value of the attractive force when it is influenced by the repulsive force, limiting the maximum value of the attractive force when subjected to the repulsive force. Taking into account the dynamic characteristics of USVs, this paper limits the maximum linear speed and maximum angular speed of USVs. For maintaining the stability of the formation, the leader moves at a constant speed, and the linear speed of the follower varies during the movement process, which may be greater than the speed of the leader, but must be smaller than the maximum linear speed.

The rest of this article is organized as follows: the APF method is described in Section 2; The formation control methods are described in Section 3; Section 4 presents the USV formation control and obstacle avoidance method; The simulation results and analysis are presented in Section 5; and Section 6 contains the conclusion.

2. Artificial Potential Filed

The APF method for path planning is a virtual force method proposed by Khatib [18]. The basic idea is to design the motion of a robot in its surrounding environment as an abstract artificial potential field. The target point generates “gravity” or “attractive force” on the mobile robot, and obstacles generate “repulsive force” on the mobile robot. Finally, the motion of the mobile robot is controlled by finding the resultant force. The path planned using an APF is generally relatively smooth and safe.

The goal point in the environment produces a gravitational potential field, guiding the USV toward it. Each obstacle in the environment produces a repulsive field, which in turn exerts a repulsive force on the USV, pushing the USV away from the obstacle. All the attractive forces produced by the goal and the repulsive forces produced by the obstacles generate a combined force, whose direction is the moving direction of the USV. A diagram of force analysis for an APF is depicted in Figure 1. F_{att} is the attractive force generated by the goal, F_{rep} is the repulsive force generated by the obstacle, and F is the combined force.

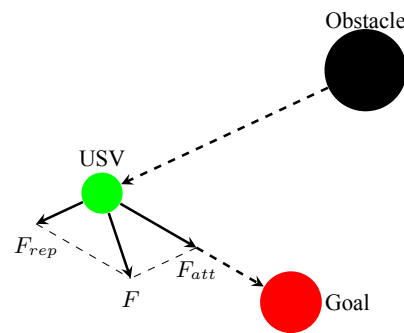


Figure 1. Diagram of the force analysis of an APF.

The potential function of the goal can be represented through

$$U_{att}(\mathbf{p}, \mathbf{p}_G) = \frac{1}{2}k_{att}\rho^2(\mathbf{p}, \mathbf{p}_G), \tag{1}$$

where $U_{att}(\mathbf{p})$ is the potential field at the position \mathbf{p} , the goal is at the position \mathbf{p}_G , $k_{att}(> 0)$ is the attractive gain, and $\rho(\mathbf{p}, \mathbf{p}_G) = \|\mathbf{p} - \mathbf{p}_G\|$ is the shortest distance between \mathbf{p} and \mathbf{p}_G .

As the USV approaches the goal position, the potential field intensity generated by Equation (1) decreases, and the field intensity becomes 0 when it reaches the goal position. The potential fields generated with two different attractive gains are shown in Figure 2.

The force \mathbf{F}_{att} generated by the goal potential field is the gradient of Equation (1),

$$\mathbf{F}_{att}(\mathbf{p}, \mathbf{p}_G) = -\nabla U_{att}(\mathbf{p}, \mathbf{p}_G) = k_{att}(\mathbf{p}_G - \mathbf{p}), \tag{2}$$

where \mathbf{F}_{att} is a vector whose direction is from \mathbf{p} to \mathbf{p}_G , ∇ is the gradient operator. The variation in the magnitude of \mathbf{F}_{att} with the distance d between the goal and the USV is illustrated in Figure 3. From Equation (2) and Figure 3, it can be observed that the force has a linear relationship with the distance when the potential field function is described using Equation (2).

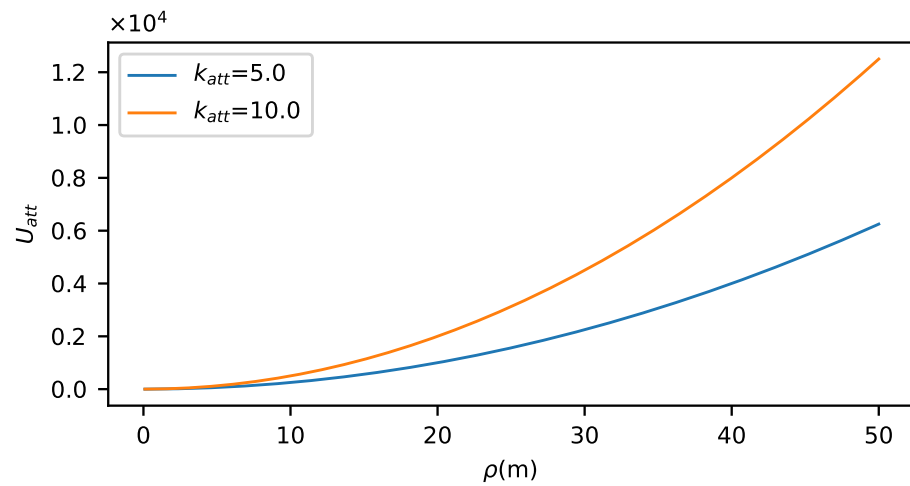


Figure 2. The potential field generated by the goal.

The potential function of the obstacle can be represented through

$$U_{rep}(\mathbf{p}, \mathbf{p}_O) = \begin{cases} \frac{1}{2}k_{rep} \left(\frac{1}{\rho(\mathbf{p}-\mathbf{p}_O)} - \frac{1}{\rho_0} \right)^2, & \rho(\mathbf{p} - \mathbf{p}_O) \leq \rho_0, \\ 0, & \rho(\mathbf{p} - \mathbf{p}_O) > \rho_0, \end{cases} \quad (3)$$

where U_{rep} is the potential field of the USV at the position \mathbf{p} , the obstacle is at the position \mathbf{p}_O , ρ_0 limits the influence range of the potential field, and $k_{rep} (> 0)$ is the repulsive gain. As the USV approaches the obstacle, the field intensity generated by Equation (3) increases rapidly.

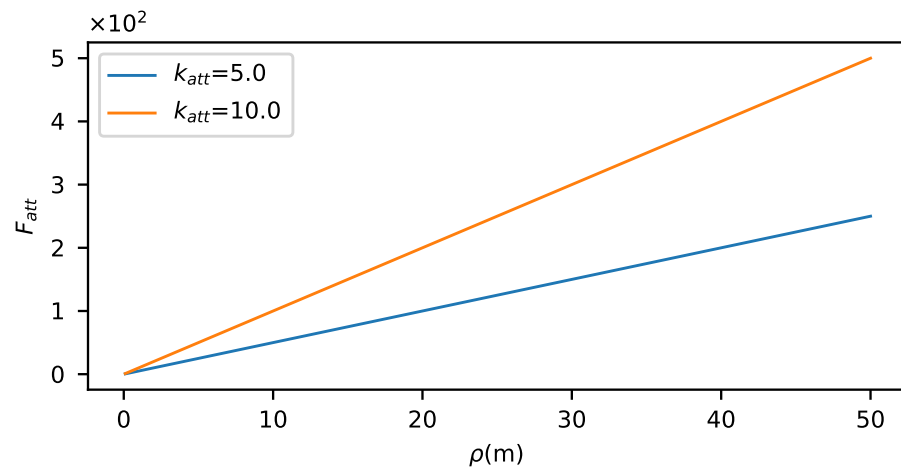


Figure 3. The force generated by the goal.

The intensity approaches infinity when $\rho(\mathbf{p} - \mathbf{p}_O)$ approaches 0. When $\rho(\mathbf{p} - \mathbf{p}_O) > \rho_0$, the field intensity is 0. The potential fields generated by the two different repulsive gains and $\rho = 1.0$ m are shown in Figure 4.

From Figure 4, it can be observed that the potential field of the obstacle decays rapidly with increasing distance, and the repulsive gains only affect the intensity of the repulsive field within a very close range of the obstacle.

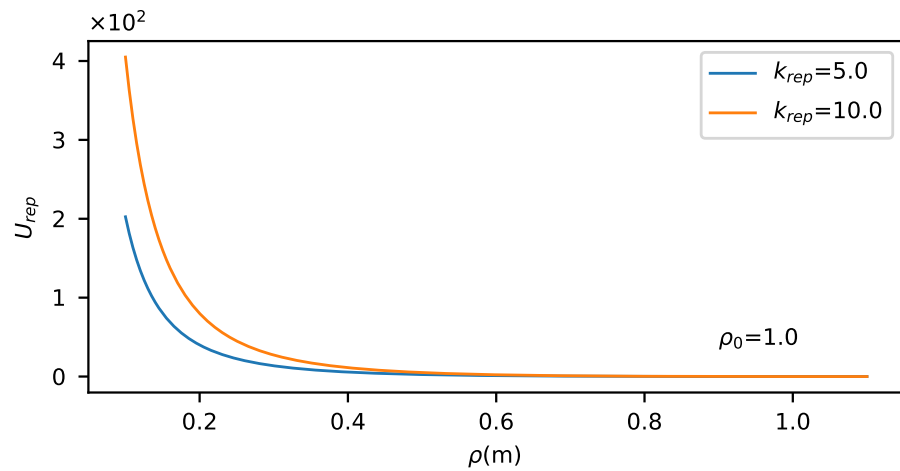


Figure 4. The potential field generated by the obstacle.

The repulsive force $F_{rep}(\mathbf{p})$ generated by the obstacle is the gradient of Equation (3),

$$F_{rep}(\mathbf{p}, \mathbf{p}_O) = -\nabla U_{rep}(\mathbf{p}, \mathbf{p}_O) = \begin{cases} k_{rep} \left(\frac{1}{\rho(\mathbf{p}_O - \mathbf{p})} - \frac{1}{\rho_0} \right) \frac{1}{\rho^2(\mathbf{p}_O - \mathbf{p})} \nabla \rho(\mathbf{p}_O - \mathbf{p}), & \rho(\mathbf{p} - \mathbf{p}_O) \leq \rho_0, \\ 0, & \rho(\mathbf{p} - \mathbf{p}_O) > \rho_0. \end{cases} \quad (4)$$

where F_{rep} is a vector whose direction is from \mathbf{p}_O to \mathbf{p} . The variation in the magnitude of F_{rep} with the distance d between the obstacle and the USV is depicted in Figure 5.

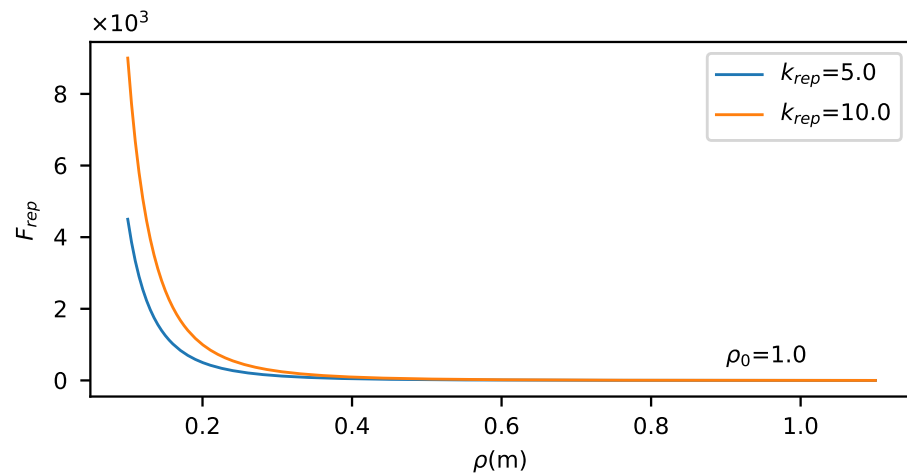


Figure 5. The force generated by the obstacle.

When the potential field is generated by one goal and multiple obstacles, the combined force $\mathbf{F}(\mathbf{p})$ received by the USV is

$$\mathbf{F}(\mathbf{p}) = \mathbf{F}_{att}(\mathbf{p}, \mathbf{p}_G) + \sum_{i=0}^{M-1} \mathbf{F}_{rep}(\mathbf{p}, \mathbf{p}_{O_i}), \quad (5)$$

where M is the number of obstacles in the potential field. The direction $\mathbf{F}(\mathbf{p})$ is the moving direction of the USV.

3. Formation Control Method

3.1. Behavior-Based Method

The behavior-based method controls the behavior of the entire formation by weighting the expected behaviors, including avoiding obstacles, maintaining the desired formation, and reaching the target point. In reality, for an USV fleet in formation, it is often necessary to simultaneously achieve multiple control objectives, such as formation maintenance and target search. Formation maintenance means that the USV fleet maintains a certain relative positional relationship when the USV fleet is moving. Target search means that the members of the formation search for the target area through the collaborative movement of the members and find the target object or location. These two control objectives have different impacts on the behavior of the formation members, so the behavior of the formation needs to be adjusted accordingly. The behavior-based method compromises multiple control objectives and weights each control behavior to enable the formation members to coordinate and complete various tasks [19,20].

3.2. Virtual Structure Method

The virtual structure method utilizes the position and attitude information of each target point to form the formation. These target points usually correspond to the points on a rigid body. Compared to other formation methods, the control concept of this method is easier to understand and more convenient to implement. However, centralized control is required and the flexibility of the formation is insufficient, which also poses significant problems in obstacle avoidance [21,22].

3.3. Graph Theory Method

The graph theory method uses a control graph to define the shape of USV formations, where each node represents an USV and the directed edges between nodes represent the relative relationship between two USVs. The distributed nature of graph theory determines that it can be used for large-scale USV formations, making it easy to handle the addition or deletion of USV nodes in occasional queues. Using graph theory to describe the formation and the relationship between USVs, facilitating the main exchange between different formations. One disadvantage is that it is mainly limited to simulation research, and the implementation is relatively complex [23,24].

3.4. Leader-Follower Method

The basic idea of the leader-follower method is that, in a group composed of multiple USVs, one USV is designated as the leader and the other USVs are its followers. The followers follow the position and orientation of the leader USV at a certain distance interval. This method can also be extended on the basis of the above description, which can, not only specify one leader, but also specify multiple leaders. However, in the control of group formation, the leader is often designated as one. According to the relative positional relationship between leaders and followers, different network topologies can be formed, which means forming different formations. In a system that employs this method to control the formation of USVs, collaboration is achieved by sharing knowledge such as the state of the leader. The advantage of the leader-follower method is that simply giving the leader's behavior or trajectory can control the behavior of the entire USV population. The main drawback is that there is no clear formation feedback in the system. For example, if the USV leader advances too quickly, the following USV may not be able to track in time. Another drawback is that if the leader fails, the entire formation cannot be maintained [24–28].

4. USV Formation Control and Obstacle Avoidance Method

In this paper, we utilize a leader-follower and virtual structure method for formation control, and use an APF for obstacle avoidance. For simplicity, we simplify the dynamic description of the USVs by limiting the maximum linear speed and maximum angular speed. The leader is moving at a constant speed. To address the issue of limited flexibility

in maintaining formation using virtual structure methods and to enhance the stability of the formation, the linear speed of the follower can be adjusted based on the distance between the follower and the object being tracked, which may be greater than the speed of the leader but must be smaller than the maximum linear speed.

The USV leader is influenced by the attractive force generated by the task target, as well as the repulsive force generated by all obstacles in the environment and other USVs in the fleet. The USV leader calculates its position and the heading angle in the next moment based on the combined direction of the attractive and repulsive force, combined with the linear speed and maximum angular speed constraints of the formation movement.

After determining the position and the heading angle of the leader in the next moment, the leader uses the virtual structure method to calculate the ideal position of each follower based on the position and the heading angle of the leader itself. The followers are attracted by the forces generated by their respective ideal positions or the target position, depending on whether they are repelled by obstacles or not, as well as the repulsive forces generated by all obstacles and the other USVs in the environment. The followers are guided by the direction of the combined forces generated by the attractive and repulsive forces. The followers calculate their heading angles in the next moment by combining the maximum linear speed and the maximum angular speed constraints during the follower's movement.

In order to quickly leave the obstacle area, this paper modifies the attractive force model of the traditional APF. We restrict the maximum magnitude of the attractive force when influenced by the repulsive force, to modify the direction of the combined force.

There are three points to note: first, the speed of the USV formation is the same as the speed of the leader, but the speed of the follower can be greater than the formation speed to meet the needs of maintaining the formation; second, the follower may be pulled by the target position or the ideal position, depending on whether they are repelled by obstacles or not; third, when a USV is subject to a repulsive force, the magnitude of its attractive force is restricted by that of the repulsive force. This restriction can impact the heading angle of the USV.

Below, we elaborate on the principles of the method proposed in this article.

4.1. Formation Representation

This article uses the body coordinate system of the leader to represent the formation. The heading direction of the leader is taken as the positive direction of the x -axis, and the y -axis coordinate direction of the leader is determined using the right hand rule. The origin O of the xy coordinate system can be specified as needed.

We represent the position of the follower i in the formation with (α_i, l_i) . α_i is the azimuth in the leader body coordinate system, and l_i is the distance between the follow i and the origin, as shown in Figure 6. The coordinate (x_i, y_i) of the follower i in the leader body coordinate system can be obtained through

$$\begin{cases} x_i &= l_i \cos(\alpha_i) \\ y_i &= l_i \sin(\alpha_i) \end{cases} \quad (6)$$

When the positions of all followers are specified, the formation of the USVs is determined.

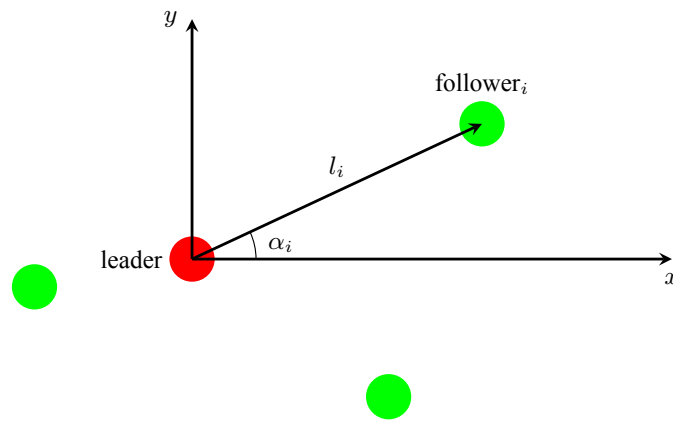


Figure 6. Formation representation in the leader body coordinate system. The red solid circle represents the leader, and the green solid circles represent the followers.

4.2. Obstacle Avoidance and Formation Update

Assume that the USV formation contains N USVs, which consist of 1 leader and $N - 1$ followers, and there are M obstacles in the task scenario. We number the USVs, the id $i(0 \leq i \leq N - 1)$ represents the i th USV, and the id of the leader is 0. We also number the obstacles, the id $j(0 \leq j \leq M - 1)$ represents the j th obstacle. Assume that \mathbf{p}_{Ii} represents the ideal position of the USV i in the world coordinate system, and \mathbf{p}_{Ai} represents the actual position of the USV i in the world coordinate system, and \mathbf{p}_{Oj} represents the position of the obstacle j in the world coordinate system.

4.2.1. The Unit Vector of the Combined Force on the Leader

The repulsive force on the leader is

$$\mathbf{F}_{rep}(\mathbf{p}_{A0}) = \sum_{i=0}^{M-1} \mathbf{F}_{rep}(\mathbf{p}_{A0}, \mathbf{p}_{O_i}) + \sum_{i=1}^{N-1} \mathbf{F}_{rep}(\mathbf{p}_{A0}, \mathbf{p}_{A_i}). \tag{7}$$

In order to quickly leave the obstacle area, we limit the maximum of the attractive force when subjected to the repulsive force to modify the direction of the combined force. We adjust the magnitude of the attractive force using

$$\mathbf{F}_{att}(\mathbf{p}_{A0}, \mathbf{p}_G) = \begin{cases} \frac{a \|\mathbf{F}_{rep}(\mathbf{p}_{A0}, \mathbf{p}_G)\|}{\|\mathbf{F}_{att}(\mathbf{p}_{A0})\|} \mathbf{F}_{att}(\mathbf{p}_{A0}, \mathbf{p}_G), & \|\mathbf{F}_{att}(\mathbf{p}_{A0}, \mathbf{p}_G)\| > \|\mathbf{F}_{rep}(\mathbf{p}_{A0})\|, \\ \mathbf{F}_{att}(\mathbf{p}_{A0}, \mathbf{p}_G) = \mathbf{F}_{att}(\mathbf{p}_{A0}, \mathbf{p}_G), & \|\mathbf{F}_{att}(\mathbf{p}_{A0}, \mathbf{p}_G)\| \leq \|\mathbf{F}_{rep}(\mathbf{p}_{A0})\|, \end{cases} \tag{8}$$

where $a(0 < a < 1.0)$ is the weighting coefficient that can modify the direction of the combined force.

Now, we can calculate the unit vector of the combined force on the leader. From Equation (5), the combined force on the leader is

$$\mathbf{F}(\mathbf{p}_{A0}) = \mathbf{F}_{att}(\mathbf{p}_{A0}, \mathbf{p}_G) + \mathbf{F}_{rep}(\mathbf{p}_{A0}). \tag{9}$$

Thus, the unit vector of $\mathbf{F}(\mathbf{p}_{A0})$ is

$$\mathbf{F}_{unit}(\mathbf{p}_{A0}) = \frac{\mathbf{F}(\mathbf{p}_{A0})}{\|\mathbf{F}(\mathbf{p}_{A0})\|}. \tag{10}$$

4.2.2. The Next Moment Position and the Heading Angle of the Leader

Assume that θ_{yaw} represents the heading angle of the USV formation, which is also the heading angle of the leader. Assume that ω_m is the maximum angular speed of the USV. The next moment heading angle θ of the leader can be obtained through

$$\theta = \arctan \left(\frac{\text{Im}(\mathbf{F}_{unit}(\mathbf{p}_{A0}))}{\text{Re}(\mathbf{F}_{unit}(\mathbf{p}_{A0}))} \right), \tag{11}$$

where $\text{Re}(\cdot)$ represents the real part, and $\text{Im}(\cdot)$ represents the imaginary part.

The heading angle difference $\Delta\theta$ between two consecutive moments is

$$\Delta\theta = \theta_{yaw} - \theta. \tag{12}$$

Update the heading angle θ_{yaw} using the maximum angular speed ω_m of the USV,

$$\theta_{yaw} = \begin{cases} \theta, & |\Delta\theta| \leq \omega_m, \\ \theta_{yaw} + \omega_m, & |\Delta\theta| > \omega_m. \end{cases} \tag{13}$$

\mathbf{p}_{I0} not only represents the ideal position of the leader but also the actual position of the next moment of the leader. In other words, $\mathbf{p}_{I0} = \mathbf{p}_{A0}$. Assume that the linear speed of the USV formation is v_f , which is a scalar. \mathbf{p}_{I0} can be obtained using the heading angles θ_{yaw} and v_f ,

$$\mathbf{p}_{I0} = \mathbf{p}_{A0} + v_f(\cos \theta_{yaw}, \sin \theta_{yaw}). \tag{14}$$

4.2.3. The Ideal Position of the Follower

Now the ideal formation position of the follower can be updated based on the position and the heading angle of the leader using the virtual structure.

The ideal position \mathbf{p}_{Ii} of the follower i can be obtained using

$$\mathbf{p}_{Ii} = \mathbf{p}_{I0} + l_i(\cos(\theta_{yaw} + \alpha_i), \sin(\theta_{yaw} + \alpha_i)). \tag{15}$$

The relationships among the formation representation (\mathbf{p}_i, l_i) in the leader body coordinate system and the leader position \mathbf{p}_{I0} and the follower position \mathbf{p}_{Ii} are shown in Figure 7.

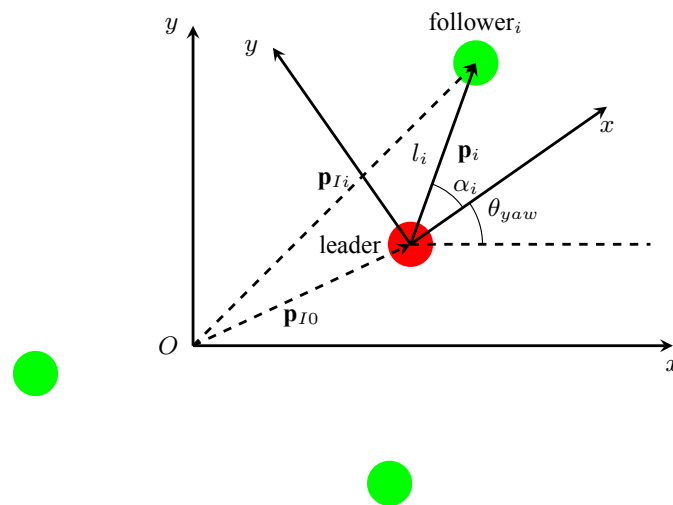


Figure 7. The relationship between the formation representations in the world coordinate system and in the leader body coordinate system. The red solid circle represents the leader, and the green solid circles represent the followers.

4.2.4. The Unit Vector of the Combined Force on the Follower

The repulsive force on the follower i is

$$\mathbf{F}_{rep}(\mathbf{p}_{Ai}) = \sum_{j=0}^{M-1} \mathbf{F}_{rep}(\mathbf{p}_{Ai}, \mathbf{p}_{Oj}) + \sum_{j=0, j \neq i}^{N-1} \mathbf{F}_{rep}(\mathbf{p}_{Ai}, \mathbf{p}_{Aj}). \quad (16)$$

We adjust the magnitude of the attractive force for the follower i through

$$\mathbf{F}_{att}(\mathbf{p}_{Ai}, \mathbf{p}_T) = \begin{cases} \frac{a \|\mathbf{F}_{rep}(\mathbf{p}_{Ai}, \mathbf{p}_T)\|}{\|\mathbf{F}_{att}(\mathbf{p}_{Ai})\|} \mathbf{F}_{att}(\mathbf{p}_{Ai}, \mathbf{p}_T), & \|\mathbf{F}_{att}(\mathbf{p}_{Ai}, \mathbf{p}_T)\| > \|\mathbf{F}_{rep}(\mathbf{p}_{Ai})\|, \\ \mathbf{F}_{att}(\mathbf{p}_{Ai}, \mathbf{p}_T) = \mathbf{F}_{att}(\mathbf{p}_{Ai}, \mathbf{p}_T), & \|\mathbf{F}_{att}(\mathbf{p}_{Ai}, \mathbf{p}_T)\| \leq \|\mathbf{F}_{rep}(\mathbf{p}_{Ai})\|. \end{cases} \quad (17)$$

where \mathbf{p}_T is the position \mathbf{p}_G of the target or the ideal position \mathbf{p}_{Ii} of the follower i based on whether it is repelled by obstacles or not.

Now, we can calculate the unit vector of the combined force on the follower. From Equation (5), we can obtain the combined force on the follower i . If the follower is repelled by some obstacles, the combined force is

$$\mathbf{F}(\mathbf{p}_{Ai}) = \mathbf{F}_{att}(\mathbf{p}_{Ai}, \mathbf{p}_T) + \mathbf{F}_{rep}(\mathbf{p}_{Ai}). \quad (18)$$

Thus, the unit vector of $\mathbf{F}(\mathbf{p}_{Ai})$ is

$$\mathbf{F}_{unit}(\mathbf{p}_{Ai}) = \frac{\mathbf{F}(\mathbf{p}_{Ai})}{\|\mathbf{F}(\mathbf{p}_{Ai})\|}. \quad (19)$$

4.2.5. The Next Moment Position and the Heading Angle of the Follower

Assume that β_i represents the heading angle of the follower i at the moment. The next moment heading angle β of the follower i can be obtained through

$$\beta = \arctan \left(\frac{\text{Im}(\mathbf{F}_{unit}(\mathbf{p}_{Ai}))}{\text{Re}(\mathbf{F}_{unit}(\mathbf{p}_{Ai}))} \right). \quad (20)$$

The heading angle difference $\Delta\beta$ between two consecutive moments is

$$\Delta\beta = \beta - \beta_i. \quad (21)$$

Update the heading angle β_i using the maximum angular speed of the USV,

$$\beta_i = \begin{cases} \beta, & |\Delta\beta| \leq \omega_m, \\ \beta_i + \omega_m, & |\Delta\beta| > \omega_m. \end{cases} \quad (22)$$

When the heading angle of the USV formation changes significantly, this has a significant impact on the position changes of the follower at the edge of the formation. For the stability of the formation, we allow the follower's linear speed to be greater than the formation speed.

The distance d_i between the follower i and the traction object is

$$d_i = \|\mathbf{p}_{Ii} - \mathbf{p}_{Ai}\|, \quad (23)$$

or

$$d_i = \|\mathbf{p}_G - \mathbf{p}_{Ai}\|, \quad (24)$$

depending on whether the follower is repelled by obstacles or not.

Assume that the maximum linear speed of the USV follower is v_m , which is a scalar. We adjust the follower's speed v_i based on d_i ,

$$v_i = \begin{cases} v_m, & d_i \geq v_m, \\ d_i, & d_i < v_m. \end{cases} \tag{25}$$

\mathbf{p}_{Ii} can be obtained using the heading direction angle β_i ,

$$\mathbf{p}_{Ii} = \mathbf{p}_{Ai} + v_i(\cos \beta_i, \sin \beta_i). \tag{26}$$

4.3. Algorithm

The formation control and obstacle avoidance algorithm is summarized in Algorithm 1.

Algorithm 1: Formation Control and Obstacle Avoidance Algorithm

Input: the goal position \mathbf{p}_G , the actual position \mathbf{p}_{Ai} of the USV i , the ideal position \mathbf{p}_{Ii} of the USV i , the position \mathbf{p}_{Oj} of the obstacle j , the formation parameters α_i and l_i , the heading direction θ_{yaw} of the formation, the formation linear speed v_f , the maximum angular speed ω_m of the USV, the maximum linear speed v_m of the follower, the attractive gain F_{att} , the repulsive gain F_{rep} , the weighting coefficient a the attractive force

- 1 **while** the leader hasn't reached the goal position or the followers hasn't reached their ideal position **do**
- 2 **if** the leader hasn't reached the goal position **then**
- 3 Compute the combined force unit vector $\mathbf{F}_{unit}(A_0)$ of the leader;
- 4 Update the heading angle θ_{yaw} of the formation according the maximum angular speed ω_m ;
- 5 Compute the ideal position \mathbf{p}_{I0} of the leader with the formation linear speed v_f and θ_{yaw} , and let $\mathbf{p}_{A0} = \mathbf{p}_{I0}$;
- 6 Compute the ideal position \mathbf{p}_{Ii} of the follower i ;
- 7 **end**
- 8 **foreach** follower i **do**
- 9 **if** the follower i hasn't reached their ideal position **then**
- 10 Update the heading direction β_i of the follower i ;
- 11 Compute the distance d_i between \mathbf{p}_{Ai} and the traction object;
- 12 Compute the linear speed v_i of the follower i according d_i and the maximum linear speed v_m of the follower;
- 13 Update the actual position \mathbf{p}_{Ai} of the follower i according v_i and β_i
- 14 **end**
- 15 **end**
- 16 **end**

5. Simulation Studies

For the sake of simplicity, we assume that USVs have the formation shown in Figure 8. The USV fleet consists of 6 USVs, with an equilateral triangle formation and three USVs evenly spaced on each edge.

The id of each USV is shown in Figure 8. The width of each USV is 0.8 m, and their length is 1.0 m. The formation parameters are shown in Table 1. Table 2 shows the performance parameters of the USVs.

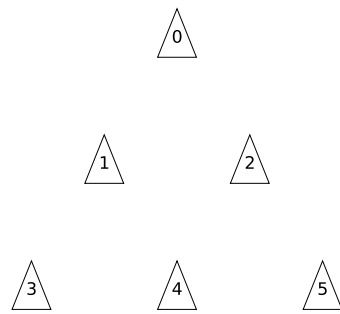


Figure 8. Formation of USVs.

Table 1. Formation parameters.

Parameters	Value	Parameters	Value
α_1	240°	l_1	3 m
α_2	300°	l_2	3 m
α_3	240°	l_3	6 m
α_4	270°	l_4	6 m
α_5	300°	l_5	$3\sqrt{3}$ m

Table 2. Performance parameters of the USV.

Parameters	Value	Parameters	Value
v_f	0.1 m/s	ω_m	15°
v_m	0.2 m/s		

5.1. Experiment without Obstacles

We first verified the formation maintenance effects of the algorithm when there is no obstacle.

In Figure 9, the black solid circle represents the starting position of the formation, the red solid circle represents the target position, the circle with numbers indicates the ideal position of the USV, and the solid triangle stands for the actual position of the USV. Figure 9b–d depicts the formations of USVs after 20, 40, and 80 iterations. From the figures, it can be observed that the USV formation reached stability after a brief adjustment.

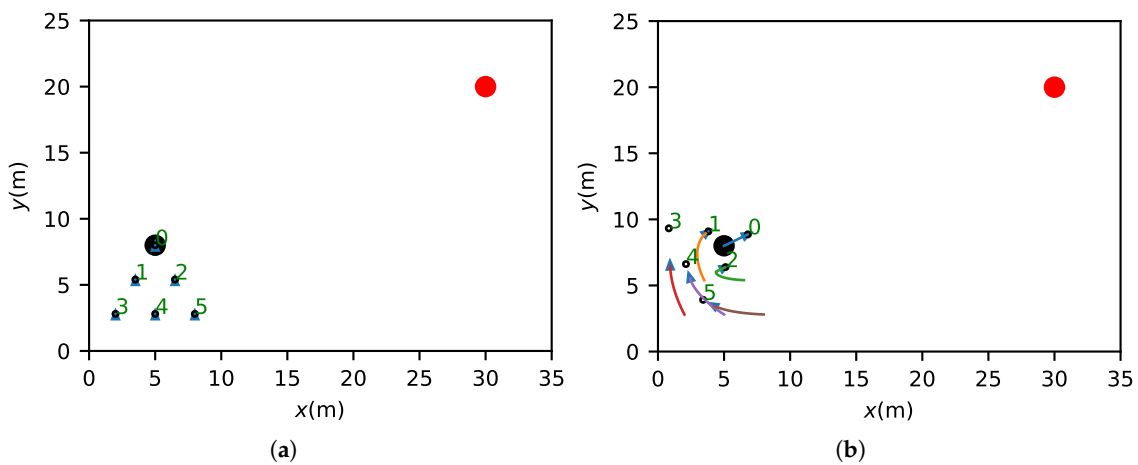


Figure 9. Cont.

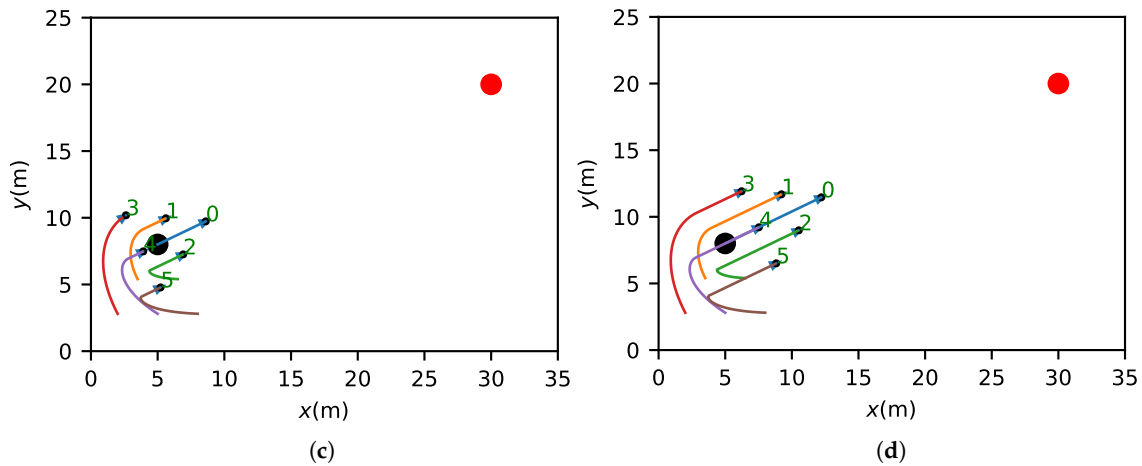


Figure 9. Formation of USVs during movement. (a) The initial formation of the USVs; (b) formation after 20 iterations; (c) formation after 40 iterations; (d) formation after 80 iterations.

5.2. Experiment with Obstacles

The parameters used in the APF approach in this simulation are shown in Table 3. The formation parameters are depicted in Table 1. The performance parameters of the USV are shown Table 2. The positions and radius of the obstacles are shown Table 4.

Table 3. APF parameters.

Parameters	Value	Parameters	Value
Goal attractive gain	5.0	Ideal position attractive gain	5.0
Obstacle repulsive gain	5.0	Limit distance	1.0 m
Attractive force weighting gain	1.0		

Table 4. Obstacle position and radius.

	Position	Radius
Obstacle 1	(15.0 m, 20.0 m)	3.0 m
Obstacle 2	(25.0 m, 10.0 m)	4.0 m
Obstacle 3	(45.0 m, 24.0 m)	1.5 m

In Figure 10, the black solid circle represents the starting position of the formation, the red solid circle indicates the target position, the circle with numbers stands for the ideal position of the USV, the solid triangle depicts the actual position of the USV, the blue solid circle represents the obstacle, and the dashed circle means the limit distance of the obstacle.

Figure 10b–f show the formations of the USVs after 150, 280, 350, 450, and 613 iterations. Figure 10f shows the final state of the USV formation after reaching its goal position. From the figures, it can be observed that the USV formation could effectively avoid obstacles and endeavored to maintain the stability of the formation during the movement.

The variation in the linear speed of the USVs over time is depicted in Figure 11. The leader moved at a constant linear speed, and the speed was 0 when it reached the target position. The linear speeds of follower 1, follower 2, and follower 5 exhibited rapid changes during specific time intervals when the USVs were maneuvering to avoid obstacles. The follower 4 encountered almost no obstacles throughout the entire process, so the time interval for rapid speed changes was very short. The time intervals during which the followers moved at their maximum speed corresponded to the adjustment periods of the formation. These can be observed from Figure 10.

In order to enhance the stability of the formation, this study allowed the maximum linear speed v_m of the followers to exceed the linear speed v_f of the leader (v_f is also the

linear speed of the formation), and the linear speed v_i of the follower i was adjusted according to Equation (25). Figure 12 shows the variation in positional errors over time when the leader moved at a linear speed 0.1 m/s, the followers moved at the maximum linear speeds of 0.1 m/s (which is equal to v_f) and 0.2 m/s (which is greater than v_f), respectively.

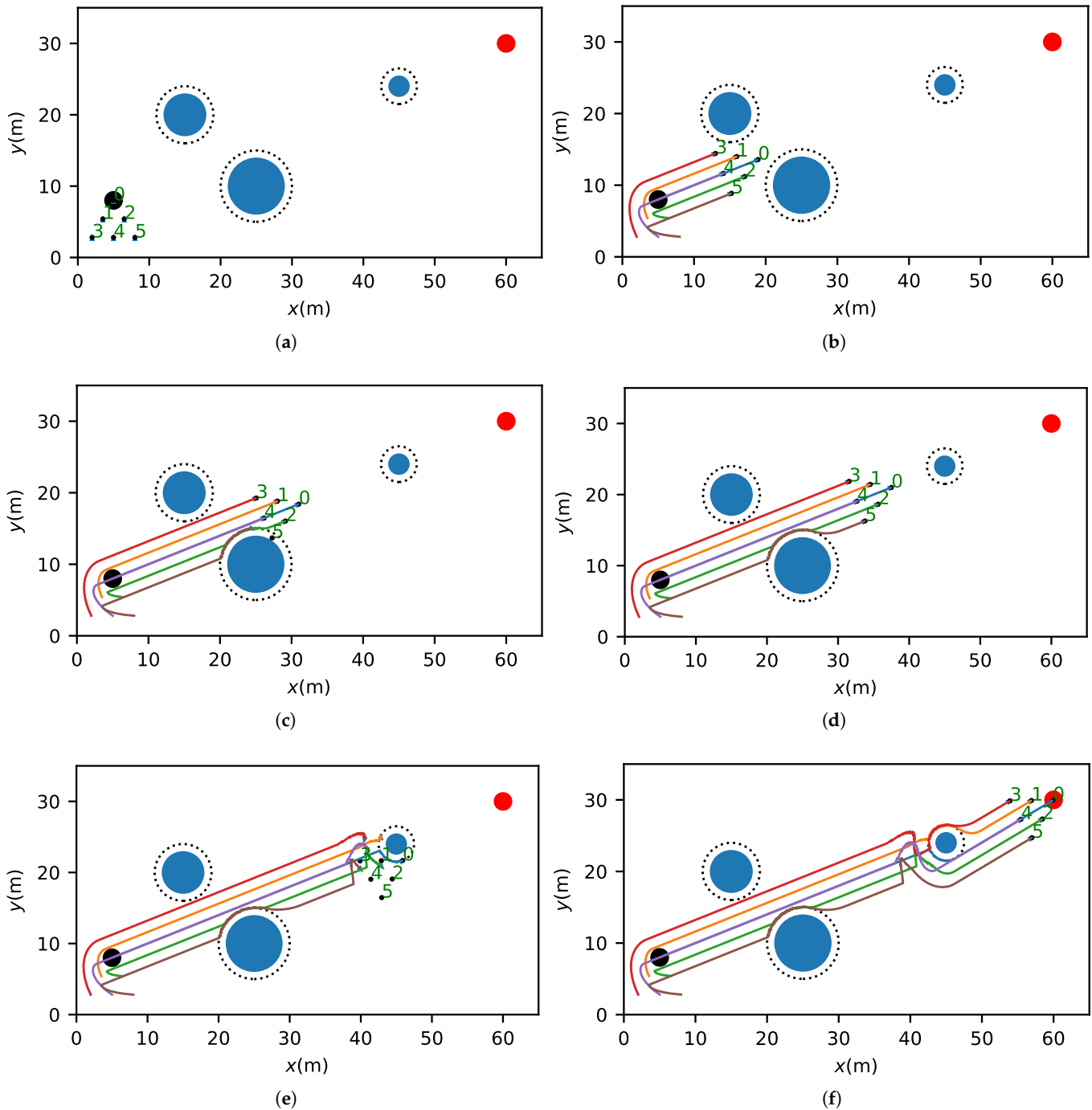


Figure 10. Formation of USVs during movement. (a) The initial formation of USVs; (b) formation after 150 iterations; (c) formation after 280 iterations; (d) formation after 350 iterations; (e) formation after 450 iterations; (f) formation after 613 iterations.

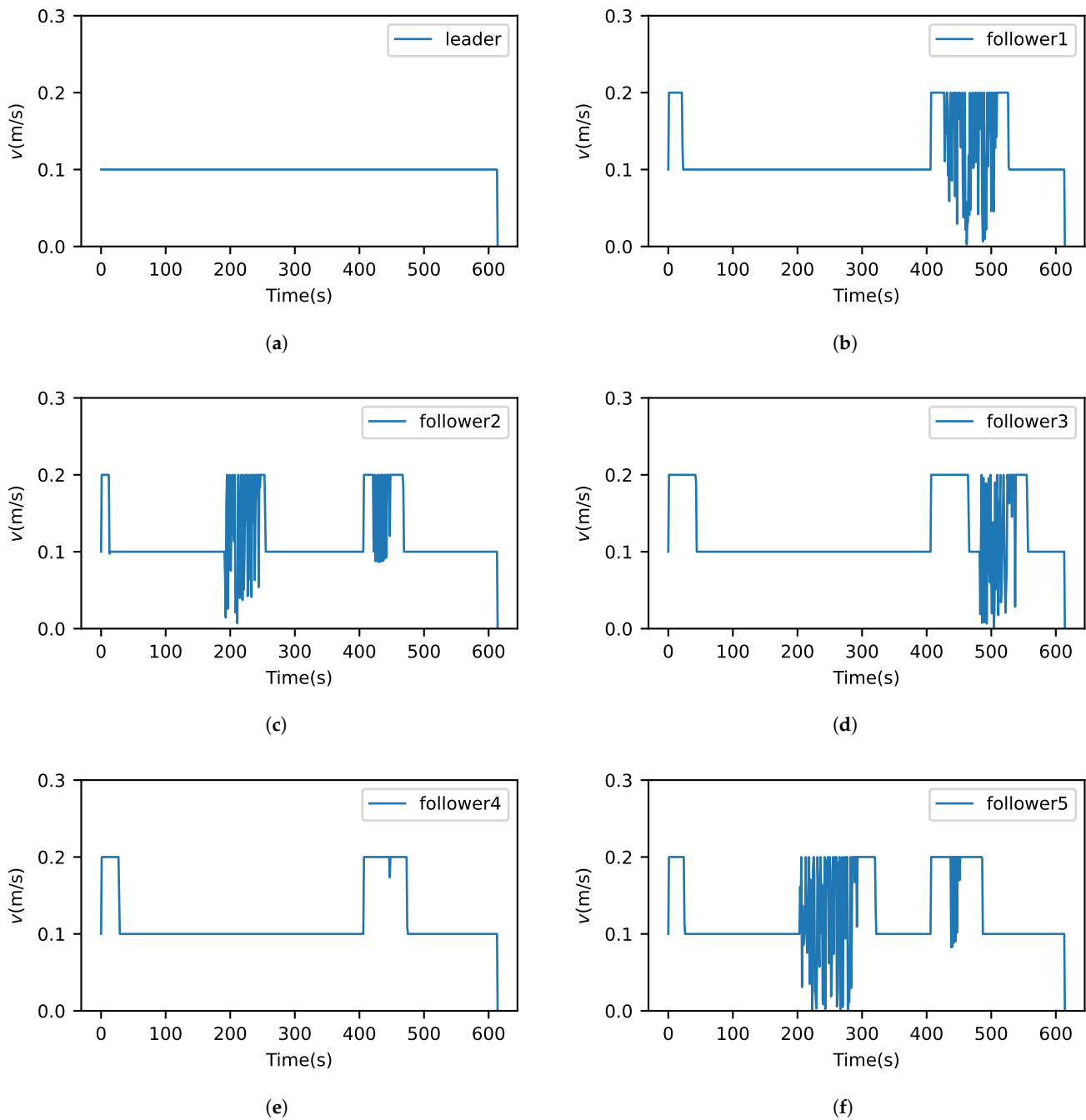


Figure 11. The varied linear speed of the USVs with respect to time. (a) Leader; (b) Follower 1; (c) Follower 2; (d) Follower 3; (e) Follower 4; (f) Follower 5.

As depicted in Figure 12, when the follower was restricted to moving at the maximum linear speed of the leader, the positional errors of the follower were large during almost the whole movement process. When the leader reached the target position, the followers required a long time to adjust to reach their respective ideal positions. When the linear speed of the follower surpassed that of the leader, the follower reached the ideal position more quickly. So when the formation changed slightly, the followers could be at the ideal positions. Under the constraints of two different maximum linear speeds, the times needed for the USV fleet to reach the target position and form a stable formation were not the same. Moreover, as evidenced by Figure 12; when the linear speed of the follower exceeded that of the leader, the time required was significantly reduced.

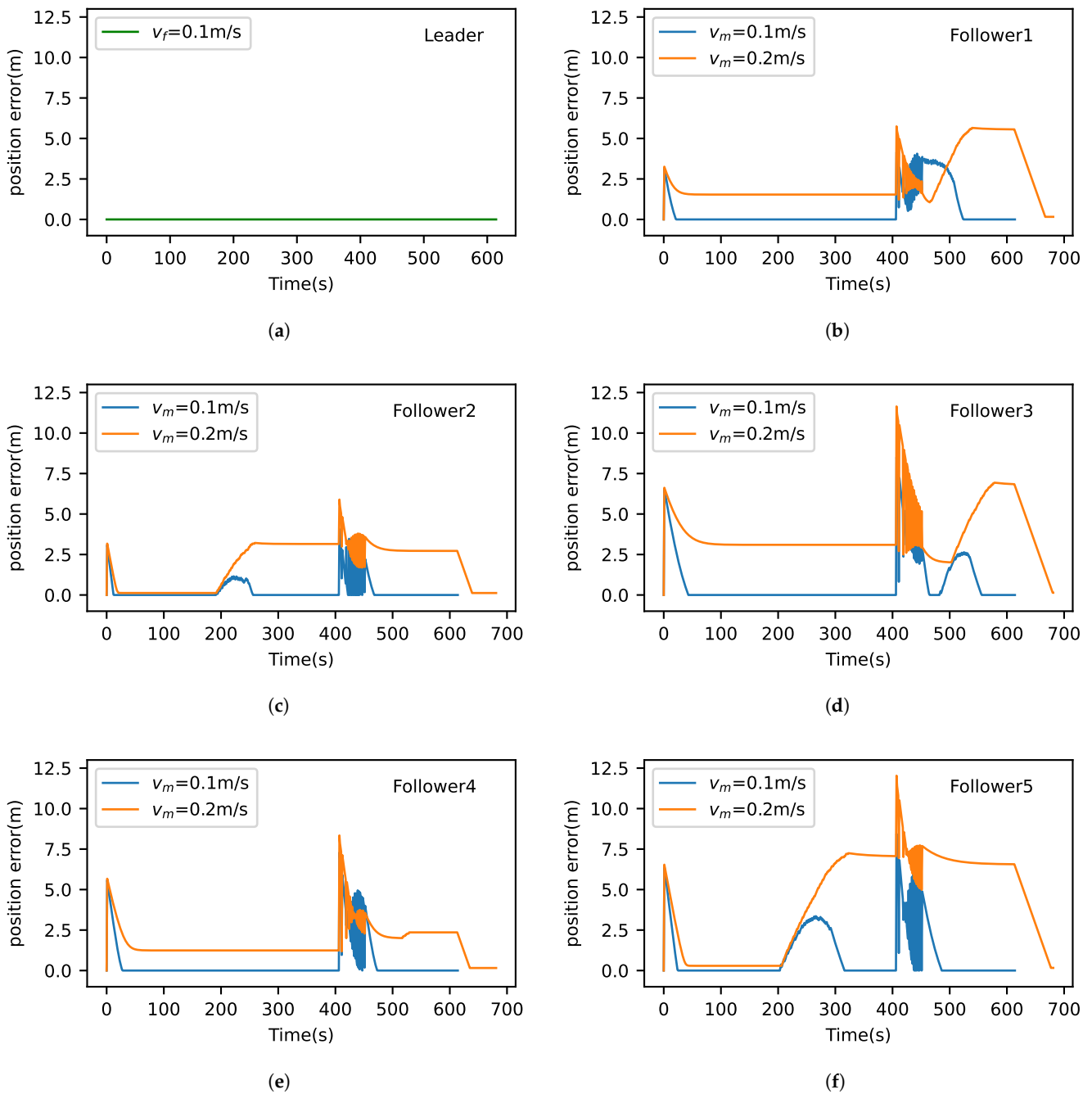


Figure 12. Comparison of positional errors of USVs at the different maximum linear speeds of 0.1 m/s and 0.2 m/s. (a) Position errors of the leader. The linear speed of the leader is $v_f = 0.1 \text{ m/s}$. $v_m = 0.1 \text{ m/s}$ and $v_m = 0.2 \text{ m/s}$ are the maximum linear speeds of the followers, not the linear speed of the leader; (b) position errors of the follower 1; (c) position errors of the follower 2; (d) position errors of the follower 3; (e) position errors of the follower 4; (f) position errors of the follower 5.

6. Conclusions

In order to seek a simple and effective method to address the challenges of formation control and obstacle avoidance for multiple USVs, this study proposed a method that combines the artificial potential field method, virtual structure method, and leader–follower method. The artificial potential field method is used to tackle the obstacle avoidance problem for USVs, while the virtual structure method is utilized to generate the ideal position of the follower within the formation. The leader–follower method is employed to

maintain the formation. The modifications were made to both the artificial potential field approach and the leader–follower scheme. To ensure the combined force deviates from obstacles and swiftly moves away from the obstacle area, the attractive force is constrained so as not to exceed the repulsive force when encountering obstacles. For effectively avoiding obstacles and maintaining formation, the followers select the target’s position or their ideal position as the reference point based on whether they are repelled by obstacles or not. Additionally, followers can adjust their linear speed depending on their distance from the reference point, without exceeding their maximum speed, to better maintain the formation. Simulation experiments showed that this method could effectively avoid obstacles and maintain the formation. However, further research is needed to address several remaining issues, including incorporating the dynamic model of the USV, considering various types of obstacles, and refining the motion trajectory of the USV to achieve smoother movements.

Author Contributions: Conceptualization, G.L. and R.Z.; methodology, G.L. and R.Z.; software N.W. and F.L.; writing—original draft preparation, G.L.; writing—review and editing, G.L. and R.Z.; visualization, N.W. and F.L. All authors have read and agreed to the published version of the manuscript.

Funding: This research was funded by Basic Research Projects for Universities of Educational Department of Liaoning Province (grant number LJKMZ20220395).

Institutional Review Board Statement: Not applicable.

Informed Consent Statement: Not applicable.

Data Availability Statement: Data is contained within the article.

Conflicts of Interest: The authors declare no conflict of interest.

References

1. Niu, Y.; Zhang, J.; Wang, Y.; Yang, H.; Mu, Y. A review of path planning algorithms for USV. In Proceedings of the 2021 International Conference on Autonomous Unmanned Systems (ICAUS 2021), Changsha, China, 24–26 September 2021.
2. Tan, G.; Zhuang, J.; Zou, J.; Wan, L. Multi-type task allocation for multiple heterogeneous unmanned surface vehicles (USVs) based on the self-organizing map. *Appl. Ocean Res.* **2022**, *126*, 103262. [\[CrossRef\]](#)
3. Wang, X.; Li, X.; Zheng, Z. Survey of developments on multi-agent formation control related problems. *Control Decis.* **2013**, *28*, 1601–1613.
4. Jin, K.; Wang, J.; Wang, H.; Liang, X.; Guo, Y.; Wang, M.; Yi, H. Soft formation control for unmanned surface vehicles under environmental disturbance using multi-task reinforcement learning. *Ocean Eng.* **2022**, *260*, 112035. [\[CrossRef\]](#)
5. MahmoudZadeh, S.; Abbasi, A.; Yazdani, A.; Wang, H.; Liu, Y. Uninterrupted path planning system for Multi-USV sampling mission in a cluttered ocean environment. *Ocean Eng.* **2022**, *254*, 111328. [\[CrossRef\]](#)
6. Miao, R.; Wang, L. Coordination of distributed unmanned surface vehicles via model-based reinforcement learning methods. *Appl. Ocean Res.* **2022**, *122*, 103106. [\[CrossRef\]](#)
7. Luo, D.; Zhang, H.; Xie, R.; Wu, S. Unmanned aerial vehicles swarm conflict based on multi-agent system. *Control Theory Appl.* **2015**, *30*, 1498–1504.
8. Tang, J.; Duan, H.; Lao, S. Swarm intelligence algorithms for multiple unmanned aerial vehicles collaboration: A comprehensive review. *Artif. Intell. Rev.* **2023**, *56*, 4295–4327. [\[CrossRef\]](#)
9. Chen, X.; Wei, X.; Xu, G. Multiple unmanned aerial vehicle decentralized cooperative air combat decision making with fuzzy situation. *J. ShangHai Jiao Tong Univ.* **2013**, *48*, 908–913, 921.
10. Jin, X.; Er, M.J. Dynamic collision avoidance scheme for unmanned surface vehicles under complex shallow sea Environments. *Ocean Eng.* **2020**, *218*, 108102. [\[CrossRef\]](#)
11. Pan, W.; Jiang, D.; Pang, Y.; Li, Y.; Zhang, Q. A multi-AUV formation algorithm combining artificial potential field and virtual structure. *Acta Armamentarii* **2017**, *38*, 326–334.
12. He, Y.; Mou, J.; Chen, L.; Zeng, Q.; Chen, P.; Zhang, S. Survey on hydrodynamic effects on cooperative control of maritime autonomous surface ships. *Ocean Eng.* **2021**, *235*, 109300. [\[CrossRef\]](#)
13. Feng, Z.; Hu, G.; Sun, Y.; Soon, J. An overview of collaborative robotic manipulation in multi-robot systems. *Annu. Rev. Control* **2020**, *49*, 113–127. [\[CrossRef\]](#)
14. Chen, H.; Wang, Y.; Xie, S.; Zhang, D.; Yan, H. Reinforcement learning-based close formation control for underactuated surface vehicle with prescribed performance and time-varying state constraints. *Ocean Eng.* **2022**, *256*, 11361. [\[CrossRef\]](#)
15. Woo, J.; Kim, N. Collision avoidance for an unmanned surface vehicle using deep reinforcement learning. *Ocean Eng.* **2020**, *199*, 107001. [\[CrossRef\]](#)

16. Kim, D.; Hirayama, K.; Park, G. Collision avoidance in multiple-ship situations by distributed local search. *J. Adv. Comput. Intell. Intell. Inform.* **2014**, *18*, 839–848. [[CrossRef](#)]
17. Ma, Y.; Zhao, Y.; Incecik, A.; Yan, X.; Li, Z. A collision avoidance approach via negotiation protocol for a swarm of USVs. *Ocean Eng.* **2021**, *224*, 108713. [[CrossRef](#)]
18. Khatib, O. Real-time obstacle avoidance for manipulators and mobile robots. *Int. J. Robotics Res.* **1986**, *5*, 90–98. [[CrossRef](#)]
19. Tan, G.; Zhuang, J.; Zou, J.; Wan, L. Coordination control for multiple unmanned surface vehicles using hybrid behavior-based method. *Ocean Eng.* **2021**, *232*, 109147. [[CrossRef](#)]
20. Nantogma, S.; Ran, W.; Yang, X.; Huang, X. Behavior-based genetic fuzzy control system for multiple USVs cooperative target protection. In Proceedings of the 2019 3rd International Symposium on Autonomous Systems (ISAS), Shanghai, China, 29–31 May 2019.
21. Li, Z.; Xian, B. Robust distributed formation control of multiple unmanned aerial vehicles based on virtual structure. *Control Theory Appl.* **2020**, *37*, 2423–2431.
22. Han, J.; Park, J.; Kim, T.; Kim, J. Precision navigation and mapping under bridges with an unmanned surface vehicle. *Auton. Robots* **2015**, *38*, 349–362. [[CrossRef](#)]
23. Lai, Y.; Li, R.; Shi, Y.; He, L. On the study of a multi-quadrotor formation control with triangular structure based on graph theory. *Control Theory Appl.* **2018**, *32*, 1530–1537.
24. Liu, Y.; Yang, Y. Formation control of multi-robot research. *Control Eng. China* **2010**, *17*, 182–186.
25. Zhang, X.; Huang, Y.; Liu, G. Research on improved leader-following formation method. *Comput. Eng. Des.* **2010**, *32*, 2547–2549.
26. Hinostroza, M.A.; Xu, H.; Soares, C.G. Experimental results of the cooperative operation of autonomous surface vehicles navigating in complex marine environment. *Ocean Eng.* **2021**, *219*, 108256. [[CrossRef](#)]
27. Dong, Y.; Chen, J. Nonlinear observer-based approach for cooperative control of networked rigid spacecraft systems. *Automatica* **2021**, *128*, 109552. [[CrossRef](#)]
28. Li, R.; Zhang, L.; Han, L.; Wang, J. Multiple vehicle formation control based on robust adaptive control algorithm. *IEEE Intell. Transp. Sys. Mag.* **2017**, *9*, 41–51. [[CrossRef](#)]

Disclaimer/Publisher’s Note: The statements, opinions and data contained in all publications are solely those of the individual author(s) and contributor(s) and not of MDPI and/or the editor(s). MDPI and/or the editor(s) disclaim responsibility for any injury to people or property resulting from any ideas, methods, instructions or products referred to in the content.